JNS PEDIATRICS

CLINICAL ARTICLE

J Neurosurg Pediatr 29:650–658, 2022

A new method for quantification of frontal retrusion and complex skull shape in metopic craniosynostosis: a pilot study of a new outcome measure for endoscopic strip craniectomy

Mustafa Sakar, MD,[1,2] Hassan Haidar,[3] Özcan Sönmez, MD,[1] Onur Erdoğan, MD,[1] Bülent Saçak, MD,[4] Yaşar Bayri, MD,[1,2] and Adnan Dağçınar, MD[1,2]

[1]Marmara University, School of Medicine, Department of Neurosurgery, Istanbul, Turkey; [2]Marmara University, Institute of Neurological Sciences, Istanbul, Turkey; [3]Marmara University, School of Medicine, Istanbul, Turkey; and [4]Marmara University, School of Medicine, Plastic and Reconstructive Surgery, Istanbul, Turkey

OBJECTIVE The objective of this study was to propose a new skull outline–based method to objectively quantify complex 3D skull shapes and frontal and supraorbital retrusion in metopic craniosynostosis using 3D photogrammetry.

METHODS A standard section from 3D photogrammetry, which represents the trigonocephalic shape, was used in this study. From the midpoint of the area of this section, half diagonals were calculated to the skull outline at 5° increments in the anterior half of the head. These half diagonals were used to create a sinusoidal curve, and the area under the sinusoidal curve (AUC) was used to represent the mathematical expression of the trigonocephalic head shape. The AUC from 0° to 180° (90° from the midline to each side) was calculated and is referred to as $AUC_{0\rightarrow180}$. The AUC from 60° to 120° (30° from the midline to each side) was also calculated and is referred to as $AUC_{60\rightarrow120}$. A total of 24 patients who underwent endoscopic strip craniectomy and 13 age- and sex-matched controls were included in the study. The AUC values obtained in patients at different time points and controls were analyzed.

RESULTS The mean preoperative $AUC_{60\rightarrow120}$ and $AUC_{0\rightarrow180}$ in the patients were significantly lower than those in control individuals. The increase in both $AUC_{60\rightarrow120}$ and $AUC_{0\rightarrow180}$ values is statistically significant at the discontinuation of helmet therapy and at final follow-up. Receiver operating characteristic curve analysis indicated that $AUC_{60\rightarrow120}$ is a more accurate classifier than $AUC_{0\rightarrow180}$.

CONCLUSIONS The proposed method objectively quantifies complex head shape and frontal retrusion in patients with metopic craniosynostosis and provides a quantitative measure for follow-up after surgical treatment. It avoids ionizing radiation exposure.

https://thejns.org/doi/abs/10.3171/2022.1.PEDS21553

KEYWORDS metopic craniosynostosis; endoscopic strip craniectomy; quantification; frontal retrusion; supraorbital retrusion; 3D photogrammetry; craniofacial

Metopic craniosynostosis (MCS) is the second most common type of single-suture synostosis, and its prevalence is speculated to be increasing.[1,2] It results from premature fusion of the metopic suture. MCS has a characteristic head shape, namely, trigonocephaly, with forehead narrowing, midline ridging, bitemporal narrowing, biparietal widening, hypotelorism, and frontal and supraorbital retrusion.[2,3]

It is suggested that the diagnosis of MCS is mostly based on examination findings.[4] However, CT is a widely used modality not only for confirmation of diagnosis but also for quantification of the pathology and outcomes. Despite efforts, an objective quantification for MCS has not yet been established. Objective quantification of trigonocephaly is essential to evaluate the severity of the preoperative malformation, for postoperative follow-up assessment, and to study associations between trigonocephaly and neurobehavioral and cognitive disorders. Almost all conceived

ABBREVIATIONS AP = anteroposterior; AUC = area under the sinusoidal curve; $AUC_{0\rightarrow180}$ = AUC from 0° to 180° (90° from the midline to each side); $AUC_{60\rightarrow120}$ = AUC from 60° to 120° (30° from the midline to each side); CVR = cranial vault remodeling; ESC = endoscopic strip craniectomy; MCS = metopic craniosynostosis; PHT = postoperative helmet therapy; rHD = relative half diagonal; ROC = receiver operating characteristic.

SUBMITTED November 29, 2021. **ACCEPTED** January 24, 2022.
INCLUDE WHEN CITING Published online March 11, 2022; DOI: 10.3171/2022.1.PEDS21553.

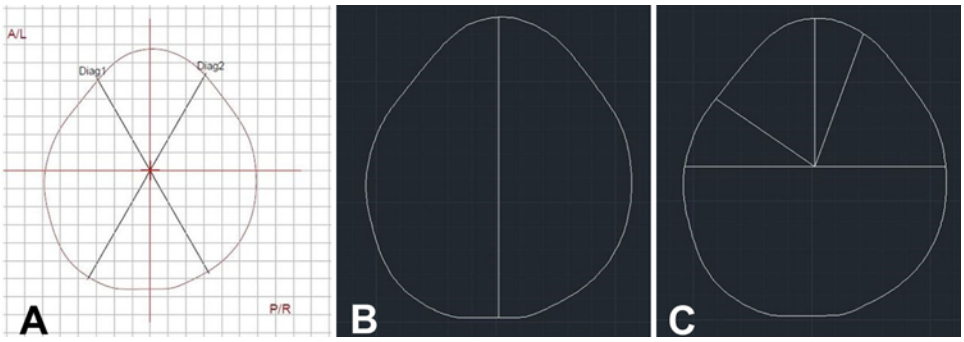

FIG. 1. A: Section 3 skull outline in 3D photogrammetry. **B and C:** The skull outline is transferred to AutoCAD while preserving the midline (B) and showing the center of this section (C), which is found by dividing the AP diameter in the midline by two, and sample half diagonals at 0°, 35°, 90°, 110°, and 180°. Figure is available in color online only.

attempts at quantifying trigonocephaly are based on the measurement of a ratio or angle between anthropometric landmarks or by measuring volumes.[5–8] Recent advancements and availability of 3D imaging with CT has led to various more sophisticated techniques, although none of them have gained popularity in clinical use.[9,10]

There are two main surgical techniques for the correction of MCS: cranial vault remodeling (CVR) and endoscopic strip craniectomy (ESC) of the metopic suture followed by postoperative helmet therapy (PHT). While CVR tries to achieve the final corrected shape during the operation due to the nature of the surgery (some regression is pronounced, and overcorrection is employed by many surgeons), suturectomy followed by PHT demands more time until the desired result is achieved, and close follow-up is of paramount importance. Taking into account the efforts to reduce ionizing radiation exposure, 3D photogrammetry becomes a very handy tool in craniosynostosis patients for follow-up and has been shown to be as effective as CT scanning for anthropometric measurements.[11]

In this study, we propose a new skull outline–based method to objectively quantify complex 3D skull shape and frontal and supraorbital retrusion in MCS using 3D photogrammetry. This method takes into account frontal retrusion, which is one of the most important indicators for aesthetic outcome in MCS. The method eliminates radiation exposure in MCS patients, and it can easily be integrated into 3D photogrammetry scanner software to automatically determine the results of the present method.

Methods

This retrospective study was approved by the local ethics committee of Marmara University.

Calculation of the Area Under the Sinusoidal Curve

Images obtained using the STARscanner laser acquisition system (Orthomerica Products) were used for this study. After adjusting images using bilateral tragions and sellions as external landmarks, 3D photogrammetric images were first divided into 10 equally distant parallel sections, with section 0 crossing bilateral tragions and the sellion, and section 10 crossing through the vertex. Then, the skull outline in section 3, which best represents the largest head circumference, trigonocephalic head shape, and frontal retrusion, was used in all measurements for a standard approach. The biparietal diameter between tragions was divided in two, and a perpendicular line crossing this midpoint was used as the midline thereafter. The image was consequently transferred to AutoCAD (Autodesk), where the rest of the calculations took place. The anteroposterior (AP) diameter was calculated along the midline, and its center represented the AP midpoint, which also corresponds to the center of the skull outline in section 3. Half diagonals were calculated from the defined center point to the skull outline at 5° increments clockwise, starting from left temporal region, designated as 0°, to the right temporal region, designated as 180° (Fig. 1). This puts the frontal midpoint at 90°. These half diagonals were then divided by the measured AP diameter to compute the relative half diagonals (rHDs), which are dimensionless and independent of a child's age and absolute skull size. The rHDs were normalized using the 0–1 normalization method. Normalized rHDs were then plotted in Microsoft Excel to create a sinusoidal curve, which was also dimensionless and represented a mathematical expression of the anterior half of the complex 3D skull shape (Fig. 2). The area under the sinusoidal curve (AUC) from 0° to 180° (90° from the midline to each side) was calculated and is referred to as $AUC_{0\rightarrow180}$. The AUC from 60° to 120° (30° from the midline to each side), which represents the maximum shape abnormality in MCS in section 3, was also calculated and is referred to as $AUC_{60\rightarrow120}$. $AUC_{0\rightarrow180}$ and $AUC_{60\rightarrow120}$ were then used for statistical analysis.

Patients and Controls

Patients with nonsyndromic single-suture MCS who underwent surgery at our tertiary center with an ESC technique between January 2018 and January 2021 were selected. Inclusion criteria for this study consisted of the following: 1) patient age younger than 6 months at the time of surgery, 2) preoperative diagnosis with CT, 3) ESC as the surgery, 4) STARscanner scanning preoperatively or early postoperatively, 5) follow-up with STARscanner until the time of PHT discontinuation or beyond, and 6) end of the PHT period. Patient sex, age at surgery, duration of PHT, and $AUC_{0\rightarrow180}$ and $AUC_{60\rightarrow120}$ at three different time points—preoperative or early postoperative (preop-

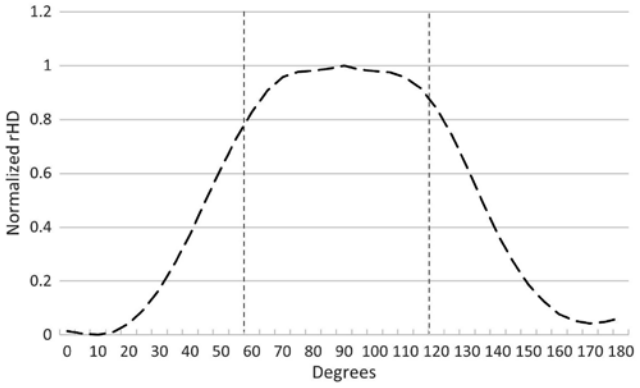

FIG. 2. Sinusoidal curve of a control group participant. The curve starts at the left temporal region at 0°, where the rHD is nearly the lowest; reaches to frontal midline at 90°, where the rHD is nearly the highest; and finishes at the right temporal region at 180°, where the rHD is again nearly the lowest.

erative $AUC_{0\rightarrow180}$ and preoperative $AUC_{60\rightarrow120}$), when the PHT was discontinued (post-PHT $AUC_{0\rightarrow180}$ and post-PHT $AUC_{60\rightarrow120}$), and at last follow-up (final $AUC_{0\rightarrow180}$ and final $AUC_{60\rightarrow120}$)—were collected. Measurements from 13 age- and sex-matched control individuals were collected. Inclusion criteria for the control cohort consisted of the following: 1) open cranial sutures without craniosynostosis; 2) scanning with STARscanner for suspicion of deformity or other head shape disorders; 3) no diagnosis of any disorders and/or syndromes that may cause head shape deformities; 4) cranial vault asymmetry index lower than 4.5, cranial index greater than 80, and head circumference between the 10th and 90th percentiles for the STARscanner measurement; and 5) normal STARscanner results. Thus, no further recommendations were given.

Surgical Technique

Patients were placed supine in a gel horseshoe headrest. After proper preparation and draping, a 3-cm-long horizontal incision was made behind the hairline bisecting the midline. A burr hole was placed in the midline, and a suturectomy was performed 8 to 10 mm to the anterior fontanelle with Kerrison rongeurs. The suturectomy was completed using a high-speed drill under an endoscopic view anteriorly, until reaching the frontonasal sutures. The dura mater and suturectomy edges were thoroughly inspected for CSF leakage and bleeding, and meticulous hemostasis was accomplished.

Helmet Protocol

PHT was usually initiated within 2 weeks after surgery following regression of scalp swelling and wound healing. Custom-made molding helmets were used to direct calvarial growth into a normal shape by limiting frontal and occipital poles to promote bifrontal expansion. Helmets were worn 23 hours a day and aimed to be used until 1 year of age during the rapid growth of the head and brain, as described in the literature.[12,13] During the PHT course, 1 or 2 helmets were used depending on serial measurements and the clinical course of the patient.

Follow-Up

Follow-up visits took place during the PHT period every 2 weeks whenever possible together with STARscanner measurements. A thorough neurological examination together with head circumference measurement was performed. PHT discontinuation was decided by the senior author (A.D.), taking into account the evolution in the trigonocephalic appearance of the patient, 3D photogrammetric imaging, and family satisfaction. After the PHT period was discontinued, follow-up visits took place at 3-month intervals. Further 3D imaging was left to family preference. An index case is presented in Fig. 3 to show the process and progress throughout the course of treatment.

Statistical Analysis

Receiver operating characteristic (ROC) curve analysis was used to study the performance of our proposed classifiers ($AUC_{0\rightarrow180}$ and $AUC_{60\rightarrow120}$) in distinguishing skull outlines of MCS patients versus control group participants.

ROC curve analysis also facilitates the determination of threshold values below which a cranium would be classified as trigonocephalic and above which the cranium would be classified as nontrigonocephalic. This analysis essentially draws a plot of sensitivity (true positive) by 1 – specificity (false positive) at every possible threshold value by dichotomizing the patients into having a trigonocephalic cranium or not. The point that provides the best balance of sensitivity and specificity is selected as the optimum cutoff value.

The overall accuracy of an ROC curve can be determined by the area under the ROC curve, which is a combined measure of sensitivity and specificity that describes the inherent validity of a diagnostic test. The maximum area under the ROC curve (1) corresponds to a diagnostic test that is perfect in group classification. On the other end of the spectrum, the minimum area under the ROC curve (0) means that the classifier incorrectly classified all subjects.

A paired-sample t-test was used to compare the mean $AUC_{60\rightarrow120}$ and $AUC_{0\rightarrow180}$ values at different time points in MCS patients and controls. Statistical analysis was performed using SPSS (version 22, IBM Corp.); $p < 0.05$ was considered statistically significant.

Results

Patient Population

A total of 24 patients (17 males and 7 females) satisfied our inclusion criteria. The mean age at surgery was 2.94 ± 0.47 months (range 2–4.5 months). The mean duration of PHT was 8.72 ± 1.66 months (range 4.6–11.4 months) (Table 1). The control group included 13 children (9 males and 4 females). Their mean age at 3D photogrammetry was 5.28 ± 4.38 months (range 2.29–17.84 months).

Area Under the Sinusoidal Curve From 60° to 120°

The differences between the mean $AUC_{60\rightarrow120}$ at three different time points of patients and the control population are shown in Fig. 4.

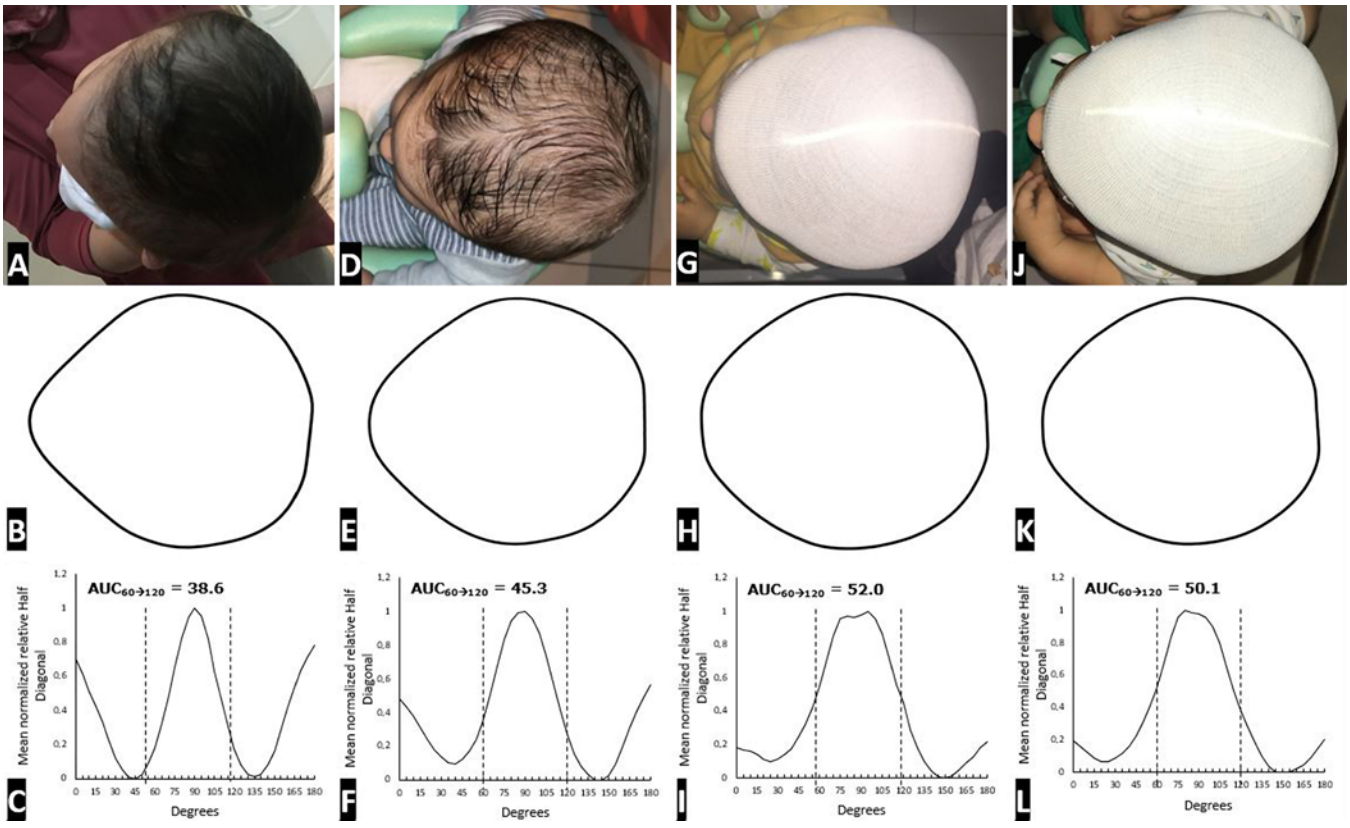

FIG. 3. Example of the process and the progress of an index patient. Although it is not relevant to calculations, 9-week postoperative data are presented for a better depiction of the course. **A–C:** Preoperatively. Top view photograph (A), skull outline in 3D photogrammetry (B), and sinusoidal curve and $AUC_{60\rightarrow120}$ value (C). **D–F:** Nine months postoperatively. Top view photograph (D), skull outline in 3D photogrammetry (E), and sinusoidal curve and $AUC_{60\rightarrow120}$ (F). **G–I:** Post-PHT after 9.1 months of helmet therapy. Top view photograph (G), skull outline in 3D photogrammetry (H), and sinusoidal curve and $AUC_{60\rightarrow120}$ value (I). **J–L:** Final follow-up at 15.2 months after surgery. Top view photograph (J), skull outline in 3D photogrammetry (K), and sinusoidal curve and $AUC_{60\rightarrow120}$ value (L). Figure is available in color online only.

The mean preoperative $AUC_{60\rightarrow120}$ was 45.65. When stratified by sex, the preoperative $AUC_{60\rightarrow120}$ was found to be higher in females (46.8) than in males (45.18); however, this difference was not statistically significant ($p = 0.190$). The mean post-PHT $AUC_{60\rightarrow120}$ and final $AUC_{60\rightarrow120}$ were 52.54 and 50.64, respectively. The mean $AUC_{60\rightarrow120}$ in the control population was 55.80. The paired-sample t-test showed that the mean 6.89 increase from preoperative $AUC_{60\rightarrow120}$ to post-PHT $AUC_{60\rightarrow120}$ and the mean 4.99 increase from preoperative $AUC_{60\rightarrow120}$ to final $AUC_{60\rightarrow120}$ were both statistically significant (both $p < 0.001$) (Table 2).

The difference between the mean $AUC_{60\rightarrow120}$ value of the control population and mean preoperative $AUC_{60\rightarrow120}$ value of the patients represents the mean initial cranial defect with which our patients presented; this averaged 10.15. The combined effect of surgery and PHT rectified on average 67.88% of the initial cranial defect; however, this value decreased to 49.16% at the final follow-up (Table 2).

Comparing the mean $AUC_{60\rightarrow120}$ of MCS patients at different time points with that of controls revealed that, despite the relative correction achieved while managing MCS patients, their preoperative $AUC_{60\rightarrow120}$, post-PHT $AUC_{60\rightarrow120}$, and final $AUC_{60\rightarrow120}$ are nonetheless consistently significantly lower than those of controls ($p < 0.001$ for the three time points) (Table 2).

TABLE 1. Patient characteristics of the study population

Variable	Mean ± SD
Age at op	2.94 ± 0.47
PHT duration, mos	8.7 ± 1.66
Follow-up duration, mos	15.08 ± 1.78

Area Under the Sinusoidal Curve From 0° to 180°

The differences between the mean $AUC_{0\rightarrow180}$ at three different time points of patients and the control population are shown in Fig. 4.

The mean preoperative $AUC_{0\rightarrow180}$ was 66.26. Female patients had higher mean preoperative $AUC_{0\rightarrow180}$ values (68.95) than male patients (65.16); however, this difference was not statistically significant ($p = 0.280$). The mean post-PHT $AUC_{0\rightarrow180}$ and final $AUC_{0\rightarrow180}$ values were 77.83

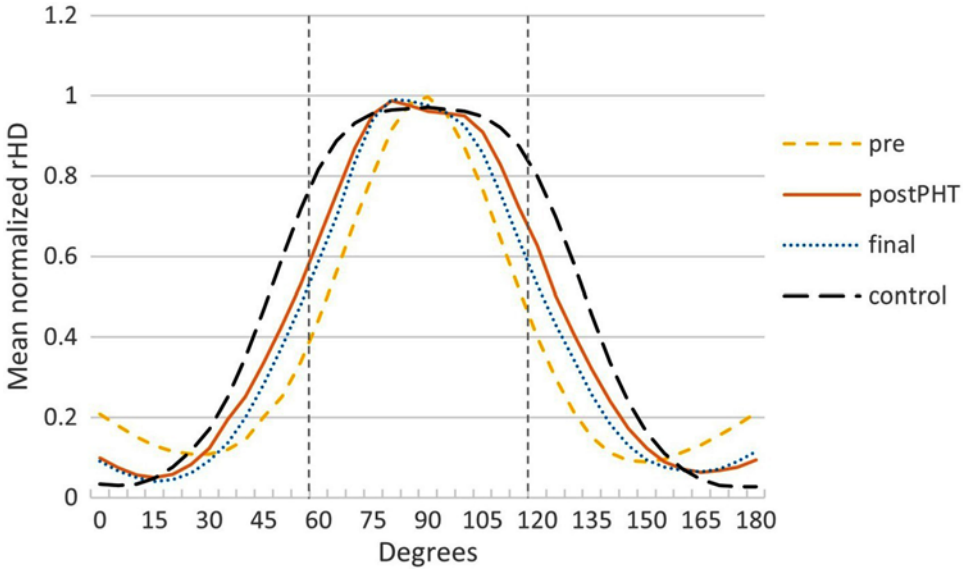

FIG. 4. The mean sinusoidal curves for the different groups. The AUCs of each curve represent the mathematical expression of the head shape in each group. The difference between control and preoperative (pre) patients represents the shape deficit in MCS patients, the difference between final and pre represents the correction with treatment, and the difference between final and control represents the residual shape deficit between final follow-up in MCS patients and controls. Figure is available in color online only.

and 72.18, respectively. The mean $AUC_{0\rightarrow180}$ in the control population was 88.10, which is significantly higher than the preoperative $AUC_{0\rightarrow180}$, post-PHT $AUC_{0\rightarrow180}$, and final $AUC_{0\rightarrow180}$ values in the patients ($p < 0.001$ for the three time points) (Table 3).

The paired-sample t-test showed that the mean 11.57 increase from preoperative $AUC_{0\rightarrow180}$ to post-PHT $AUC_{0\rightarrow180}$ and the mean 6.59 increase from preoperative $AUC_{0\rightarrow180}$ to final $AUC_{0\rightarrow180}$ were both statistically significant ($p < 0.001$ and $p = 0.031$, respectively) (Table 3).

Relative to the mean initial $AUC_{0\rightarrow180}$ cranial defect measured preoperatively as 22.44, surgical intervention followed by completion of PHT resulted in an average skull outline correction of 52.94%; however, this value regressed to 27.11% at the final follow-up (Table 3).

ROC Curve Analysis

The area under the ROC curve of the $AUC_{0\rightarrow180}$ and that of the $AUC_{60\rightarrow120}$ were 0.978 ($p < 0.001$, 95% CI 0.938–1.00) and 1.000 ($p < 0.001$, 95% CI 1.00–1.00), respectively. These findings not only indicate that $AUC_{60\rightarrow120}$ is more accurate than $AUC_{0\rightarrow180}$ as a classifier to distinguish between skull outlines of patients with MCS versus control participants but also suggest that $AUC_{60\rightarrow120}$ is seemingly a perfect diagnostic test (Fig. 5). Additionally, based on the same ROC analysis, the following cutoff values are

TABLE 2. Descriptive analysis of $AUC_{60\rightarrow120}$ values

Variable	Value	p Value
Preop $AUC_{60\rightarrow120}$	45.65 ± 2.71 (37.94 to 49.22)	<0.001*
Post-PHT $AUC_{60\rightarrow120}$	52.54 ± 2.17 (45.80 to 55.35)	<0.001*
Final $AUC_{60\rightarrow120}$	50.64 ± 1.61 (47.33 to 52.44)	<0.001*
Control $AUC_{60\rightarrow120}$	55.80 ± 2.01 (52.18 to 58.74)	
Δpreop to post-PHT $AUC_{60\rightarrow120}$	6.89 ± 3.01 (0.89 to 13.24)	<0.001
Δpreop to final $AUC_{60\rightarrow120}$	4.99 ± 3.15 (1.33 to 10.55)	<0.001
Δpost-PHT to final $AUC_{60\rightarrow120}$	−1.56 ± 1.40 (−3.65 to 1.54)	0.003
% correction at PHT discontinuation†	67.88%	
% correction at final follow-up‡	49.16%	

Mean values are presented as the mean ± SD (range).
* The mean $AUC_{60\rightarrow120}$ value is significantly less than that in the control population ($p < 0.001$).
† Calculated as follows: (post-PHT $AUC_{60\rightarrow120}$ − preoperative $AUC_{60\rightarrow120}$)/(control $AUC_{60\rightarrow120}$ − preoperative $AUC_{60\rightarrow120}$) × 100.
‡ Calculated as follows: (final $AUC_{60\rightarrow120}$ − preoperative $AUC_{60\rightarrow120}$)/(control $AUC_{60\rightarrow120}$ − preoperative $AUC_{60\rightarrow120}$) × 100.

TABLE 3. Descriptive analysis of $AUC_{0\rightarrow180}$ values

Variable	Value	p Value
Preop $AUC_{0\rightarrow180}$	66.26 ± 7.67 (55.50 to 84.29)	<0.001*
Post-PHT $AUC_{0\rightarrow180}$	77.83 ± 7.33 (67.08 to 94.62)	<0.001*
Final $AUC_{0\rightarrow180}$	72.18 ± 4.15 (65.26 to 78.07)	<0.001*
Control $AUC_{0\rightarrow180}$	88.10 ± 7.75 (72.66 to 100.41)	
Δpreop to post-PHT $AUC_{0\rightarrow180}$	11.57 ± 11.52 (−14.28 to 34.03)	<0.001
Δpreop to final $AUC_{0\rightarrow180}$	6.59 ± 9.26 (−7.18 to 22.26)	0.031
Δpost-PHT to final $AUC_{0\rightarrow180}$	−4.70 ± 4.99 (−12.13 to 5.11)	0.008
% correction at PHT discontinuation†	52.94%	
% correction at final follow-up‡	27.11%	

Mean values are presented as the mean ± SD (range).
* The mean $AUC_{0\rightarrow180}$ value is significantly less than that of the control population ($p < 0.001$).
† Calculated as follows: (post-PHT $AUC_{0\rightarrow180}$ − preoperative $AUC_{0\rightarrow180}$)/(control $AUC_{0\rightarrow180}$ − preoperative $AUC_{0\rightarrow180}$) × 100.
‡ Calculated as follows: final $AUC_{0\rightarrow180}$ − preoperative $AUC_{0\rightarrow180}$)/(control $AUC_{0\rightarrow180}$ − preoperative $AUC_{0\rightarrow180}$) × 100.

proposed, below which a skull outline may be classified as metopic: 50.7 for $AUC_{60\rightarrow120}$ (100% sensitivity, 100% specificity) and 78.66 for $AUC_{0\rightarrow180}$ (95.8% sensitivity and 92.3% specificity).

Discussion

Surgical treatment of MCS consists of two main techniques: ESC of the metopic suture followed by PHT and open CVR. In the late 1990s, ESC was suggested to have comparable results to CVR while providing additional advantages such as reduced morbidity; decreased operative time, blood loss, and hospital stays; and limited scars.[14] More recently, it was also suggested that improvement continues long after discontinuation of PHT, and results of the two techniques are equivalent in long-term follow-

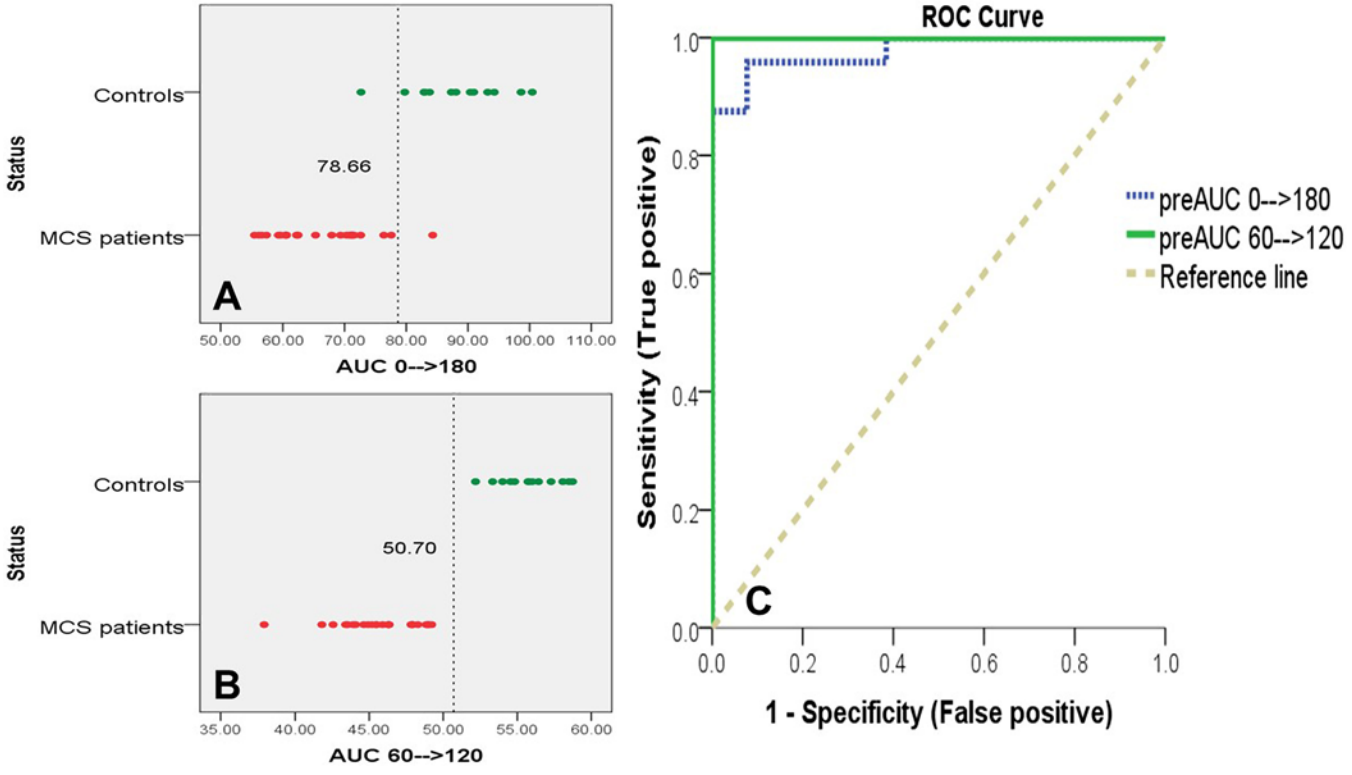

FIG. 5. A: Scatterplot of $AUC_{0\rightarrow180}$ stratified by the status of the subject with a vertical reference line at 78.66 representing the proposed threshold. **B:** Scatterplot of $AUC_{60\rightarrow120}$ stratified by the status of the subject with a vertical reference line at 50.7, representing the proposed threshold. **C:** ROC curve for classification of metopic synostosis versus normal cranium outlines by using the $AUC_{0\rightarrow180}$ (*dotted blue line*) and $AUC_{60\rightarrow120}$ (*solid green line*). Figure is available in color online only.

up.[15,16] Today, the surgical technique of choice depends primarily on the child's age at presentation, training and preference of the surgeon, and preference of the family. CVR has the advantage of achieving the final desired head shape during the operation due to the nature of the surgery, although a regression over time is debated.[17] On the other hand, ESC relies on the rapid growth of the head in the 1st year of life, which is directed using custom-molded helmets as described in the literature.[14] This puts great importance on serial imaging and quantification for patients who undergo ESC followed by PHT.

Although several quantification methods have been introduced to quantify the complex head shapes in MCS, each has its own limitations. Measuring a distance or an angle between anatomical or anthropometric landmarks is among the earliest versions of this quantification effort in MCS. The interfrontal angle is one of the most common methods that uses anatomical landmarks.[6] Likewise, similar methods are reported, which mainly depend on an angle between orbital landmarks and the most anterior part of the cranium.[18–20] These methods have common shortcomings, as they focus on the anatomy of the anterior cranial base, while evaluation of frontal and supraorbital retrusion that gives the patient actual trigonocephalic appearance is not considered. They may also have orientation difficulties depending on the technique of axial CT imaging that can be oriented in different planes, such as Frankfort horizontal or sellar nasion planes.[18] Measuring distances between anatomical landmarks, including intercanthal width, cranial breadth, and facial and frontal width, are also described extensively.[21–23] However, with the advances in imaging technology, 3D renderings of CT images have become available. This allowed for more sophisticated methods, which were thought to produce more accurate results for the stratification and classification of the dysmorphology than linear distance–based indices.[10] The use of skull outline methods was also described using both CT and 3D photogrammetry, although some of them are highly complicated for use in daily clinical practice.[9,10,24]

Older techniques that use CT images for evaluation expose children to significant amounts of radiation. Children are more vulnerable to the adverse effects of radiation exposure than adults, not only because they are more sensitive, but also because imaging with CT results in a higher effective dose with the same settings.[25] Low-dose CT imaging protocols revealed that up to a 40% decrease in radiation doses did not compromise the diagnostic quality for 3D evaluation.[26,27] However, the necessity of CT imaging in the diagnosis and/or postoperative management of single-suture craniosynostosis is a much debated subject.[4,28,29] Consistent with the "as low as reasonably achievable" principle, it is our belief that follow-up of craniosynostosis patients with CT is redundant.

The use of 3D photogrammetry avoids radiation exposure and thus provides a unique tool for serial imaging to monitor the development and progress in head shape. On the other hand, it is a relatively new technique, and it comes with its own set of limitations. There are reports on distance and angle measurements with 3D photogrammetry,[30,31] but this modality does not show bony structures, which may limit these types of measurements regarding orbits and the cranial base. It allows for composite and superimposed recreation of 3D head shape contours, but these contours do not give quantified information and they are rather qualitative assessments.[24,32] The present method incorporates 3D imaging, hence eliminating radiation exposure as suggested in the literature,[4,9,28,29] while providing quantification of the skull dysmorphology associated with MCS. Moreover, it is focused on frontal and supraorbital retrusion, which are fundamental aspects of the final aesthetic outcomes in MCS. We did not use any CT imaging for the evaluation of trigonocephalic head shape at any time point in any patient postoperatively.

The described method utilizes 3D photogrammetric images that are already in clinical use and does not necessitate further workup, as the methodology for 3D photogrammetry is already suggested to be reliable.[8,33] Several measures are considered. We started from the left temporal region and finished at the right temporal region, crossing the anterior midline, and half diagonals are measured every 5°. Consequently, this method incorporates the entire complex anterior surface features into the final measurement. Dividing these half diagonals by the actual AP distance gives us rHDs, which are dimensionless measurements. This allows comparing not only measurements of different patients or controls with each other but also measurements in the same patient at different time points. The sinusoidal curve generated and the AUC do not have any kind of dimension; rather, they are mathematical expressions of the head shape. Although we used AutoCAD, laser acquisition systems are readily capable of measuring half diagonals and AP diameters. The method can easily be integrated into photogrammetry scanner software to automatically determine AUC values; rHDs can be measured at every single degree from 0° to 180° to obtain a better resolution in AUC values.

The most temporal parts of the sinusoidal curves seem to provide no information about the trigonocephalic shape (Fig. 4), although this overall shape is the result of extreme narrowing in the frontal midline and a continuous widening in the parietal areas. This led us to define a second AUC, from 60° to 120° (30° from the midline to each side), which represents the most trigonocephalic abnormality discriminating part of the sinusoidal curve. Even though both AUCs ($AUC_{0\rightarrow180}$ and $AUC_{60\rightarrow120}$) showed a significant difference between controls and preoperative head shapes, and between preoperative and postoperative final head shapes, ROC curve analysis indicated that $AUC_{60\rightarrow120}$ is more accurate than $AUC_{0\rightarrow180}$ as a classifier to distinguish between skull outlines of MCS patients versus control participants.

The described method provides a percentage of the correction achieved, but it is obvious that the relation between the percentage correction and actual trigonocephalic shape correction is not linear. This nonlinear relation makes it difficult to set a proper stratification threshold for patients preoperatively in terms of the severity of the disorder. However, ROC curve analysis was able to propose cutoff values below which a skull outline may be classified as metopic. Studies with a greater number of patients may provide further data that can be used for stratification.

It was also suggested that lateral orbital improvement continues long after discontinuation of PHT and a slow improvement in head shape takes place in long-term follow-up after ESC and PHT.[16,24] Our mean final follow-up duration was 15.2 months, which is a relatively short period. Longer-term follow-up may reveal the nature of this nonlinear relation between percentage correction and shape correction, thus allowing stratifications and classification of the outcomes. Nonetheless, the present method successfully differentiates between normal and metopic head shapes, quantifies cranial shape deficit, and presents a gradual percentage correction of this deficit after ESC and PHT.

Limitations

This retrospective study has several limitations. The limited number of patients included in this study allowed differentiation of metopic head shapes from controls but prohibited stratification of metopic patients in terms of severity of the disorder. In addition, it is not possible to define the nature of a nonlinear relation between percentage correction that is shown with AUC values and the actual shape correction of patients. This type of assessment may need longer-term follow-ups, since minimal AUC progress may end up with a more prominent shape correction and a more prominent satisfaction about general aesthetic appearance, years after surgery.

Conclusions

Quantification of complex head shape and frontal and supraorbital retrusion in MCS is of paramount importance after ESC and PHT. Three-dimensional photogrammetry avoids ionizing radiation exposure and allows for serial imaging and close follow-up after surgical treatment. The proposed method objectively quantifies complex head shape and both frontal and supraorbital retrusion while avoiding radiation exposure in MCS patients. It also provides a quantitative measure for follow-up after surgical treatment. Using a larger number of patients, the described method can be utilized to propose cutoff values for the stratification of preoperative MCS patients according to the degree of severity of the skull dysmorphology at presentation and even of postoperative outcomes according to the extent of correction realized.

References

1. Di Rocco F, Arnaud E, Renier D. Evolution in the frequency of nonsyndromic craniosynostosis. *J Neurosurg Pediatr*. 2009;4(1):21-25.
2. van der Meulen J. Metopic synostosis. *Childs Nerv Syst*. 2012;28(9):1359-1367.
3. Birgfeld CB, Heike CL, Saltzman BS, Hing AV. Clinical characteristics and surgical decision making for infants with metopic craniosynostosis in conjunction with other congenital anomalies. *Plast Reconstr Surg Glob Open*. 2013;1(7):e62.
4. Schweitzer T, Böhm H, Meyer-Marcotty P, Collmann H, Ernestus RI, Krauß J. Avoiding CT scans in children with single-suture craniosynostosis. *Childs Nerv Syst*. 2012;28(7):1077-1082.
5. Farber SJ, Nguyen DC, Skolnick GB, Naidoo SD, Smyth MD, Patel KB. Anthropometric outcome measures in patients with metopic craniosynostosis. *J Craniofac Surg*. 2017;28(3):713-716.
6. Kellogg R, Allori AC, Rogers GF, Marcus JR. Interfrontal angle for characterization of trigonocephaly: part 1: development and validation of a tool for diagnosis of metopic synostosis. *J Craniofac Surg*. 2012;23(3):799-804.
7. Wang JY, Dorafshar AH, Liu A, Groves ML, Ahn ES. The metopic index: an anthropometric index for the quantitative assessment of trigonocephaly from metopic synostosis. *J Neurosurg Pediatr*. 2016;18(3):275-280.
8. McKay DR, Davidge KM, Williams SK, et al. Measuring cranial vault volume with three-dimensional photography: a method of measurement comparable to the gold standard. *J Craniofac Surg*. 2010;21(5):1419-1422.
9. Kronig ODM, Kronig SAJ, Vrooman HA, Veenland JF, Van Adrichem LNA. New method for quantification of the relative severity and (a)symmetry of isolated metopic synostosis. *Int J Oral Maxillofac Surg*. 2021;50(11):1477-1484.
10. Ruiz-Correa S, Starr JR, Lin HJ, et al. New severity indices for quantifying single-suture metopic craniosynostosis. *Neurosurgery*. 2008;63(2):318-325.
11. Mendonca DA, Naidoo SD, Skolnick G, Skladman R, Woo AS. Comparative study of cranial anthropometric measurement by traditional calipers to computed tomography and three-dimensional photogrammetry. *J Craniofac Surg*. 2013;24(4):1106-1110.
12. Jimenez DF, Barone CM, McGee ME, Cartwright CC, Baker CL. Endoscopy-assisted wide-vertex craniectomy, barrel stave osteotomies, and postoperative helmet molding therapy in the management of sagittal suture craniosynostosis. *J Neurosurg*. 2004;100(5 Suppl Pediatrics):407-417.
13. Sgouros S, Hockley AD, Goldin JH, Wake MJ, Natarajan K. Intracranial volume change in craniosynostosis. *J Neurosurg*. 1999;91(4):617-625.
14. Jimenez DF, Barone CM. Endoscopic craniectomy for early surgical correction of sagittal craniosynostosis. *J Neurosurg*. 1998;88(1):77-81.
15. Ha AY, Skolnick GB, Chi D, et al. School-aged anthropometric outcomes after endoscopic or open repair of metopic synostosis. *Pediatrics*. 2020;146(3):e20200238.
16. Jimenez DF, McGinity MJ, Barone CM. Endoscopy-assisted early correction of single-suture metopic craniosynostosis: a 19-year experience. *J Neurosurg Pediatr*. 2018;23(1):61-74.
17. Fearon JA, Ditthakasem K, Chan WNJ, Herbert M. Long-term growth following trigonocephaly repairs: are overcorrections necessary? *Plast Reconstr Surg*. 2020;145(3):583e-590e.
18. Nguyen DC, Patel KB, Skolnick GB, et al. Are endoscopic and open treatments of metopic synostosis equivalent in treating trigonocephaly and hypotelorism? *J Craniofac Surg*. 2015;26(1):129-134.
19. Oi S, Matsumoto S. Trigonocephaly (metopic synostosis). Clinical, surgical and anatomical concepts. *Childs Nerv Syst*. 1987;3(5):259-265.
20. Beckett JS, Chadha P, Persing JA, Steinbacher DM. Classification of trigonocephaly in metopic synostosis. *Plast Reconstr Surg*. 2012;130(3):442e-447e.
21. Kolar JC, Salter EM. Preoperative anthropometric dysmorphology in metopic synostosis. *Am J Phys Anthropol*. 1997;103(3):341-351.
22. Fearon JA, Ruotolo RA, Kolar JC. Single sutural craniosynostoses: surgical outcomes and long-term growth. *Plast Reconstr Surg*. 2009;123(2):635-642.
23. Posnick JC, Lin KY, Chen P, Armstrong D. Metopic synostosis: quantitative assessment of presenting deformity and surgical results based on CT scans. *Plast Reconstr Surg*. 1994;93(1):16-24.
24. Pressler MP, Hallac RR, Geisler EL, Seaward JR, Kane AA. Comparison of head shape outcomes in metopic synostosis

using limited strip craniectomy and open vault reconstruction techniques. *Cleft Palate Craniofac J*. 2021;58(6):669-677.
25. Brenner D, Elliston C, Hall E, Berdon W. Estimated risks of radiation-induced fatal cancer from pediatric CT. *AJR Am J Roentgenol*. 2001;176(2):289-296.
26. Cohnen M, Fischer H, Hamacher J, Lins E, Kötter R, Mödder U. CT of the head by use of reduced current and kilovoltage: relationship between image quality and dose reduction. *AJNR Am J Neuroradiol*. 2000;21(9):1654-1660.
27. Craven CM, Naik KS, Blanshard KS, Batchelor AG, Spencer JA. Multispiral three-dimensional computed tomography in the investigation of craniosynostosis: technique optimization. *Br J Radiol*. 1995;68(811):724-730.
28. Binning M, Ragel B, Brockmeyer DL, Walker ML, Kestle JR. Evaluation of the necessity of postoperative imaging after craniosynostosis surgery. *J Neurosurg*. 2007;107(1)(suppl):43-45.
29. Fearon JA, Singh DJ, Beals SP, Yu JC. The diagnosis and treatment of single-sutural synostoses: are computed tomographic scans necessary? *Plast Reconstr Surg*. 2007;120(5):1327-1331.
30. Gociman B, Agko M, Blagg R, Garlick J, Kestle JR, Siddiqi F. Endoscopic-assisted correction of metopic synostosis. *J Craniofac Surg*. 2013;24(3):763-768.
31. Ramsey JA, Stevens PM, Wurdeman SR, Bonfield CM. Quantifying orthotic correction of trigonocephaly using optical surface scanning. *J Craniofac Surg*. 2021;32(5):1727-1733.
32. Schulz M, Liebe-Püschel L, Seelbach K, et al. Quantitative and qualitative comparison of morphometric outcomes after endoscopic and conventional correction of sagittal and metopic craniosynostosis versus control groups. *Neurosurg Focus*. 2021;50(4):E2.
33. Heike CL, Cunningham ML, Hing AV, Stuhaug E, Starr JR. Picture perfect? Reliability of craniofacial anthropometry using three-dimensional digital stereophotogrammetry. *Plast Reconstr Surg*. 2009;124(4):1261-1272.

Disclosures

The authors report no conflict of interest concerning the materials or methods used in this study or the findings specified in this paper.

Author Contributions

Conception and design: Sakar, Haidar, Saçak, Dağçınar. Acquisition of data: Sakar, Haidar, Sönmez, Erdoğan. Analysis and interpretation of data: Sakar, Sönmez, Erdoğan. Drafting the article: Sakar, Haidar, Erdoğan, Saçak, Dağçınar. Critically revising the article: Sakar, Haidar, Saçak, Bayri, Dağçınar. Reviewed submitted version of manuscript: Sakar. Approved the final version of the manuscript on behalf of all authors: Sakar. Statistical analysis: Haidar, Erdoğan. Administrative/technical/material support: Sakar, Saçak, Bayri, Dağçınar. Study supervision: Sakar, Saçak, Dağçınar.

Supplemental Information

Previous Presentations

This study was presented as an oral presentation excluding receiver operating characteristic curve analysis at the 34th Scientific Congress of the Turkish Neurosurgical Society, September 30–October 3, 2021, held virtually.

Correspondence

Mustafa Sakar: Marmara University, School of Medicine, Istanbul, Turkey. docmsakar@gmail.com.